Investigation of storm track characteristics in a regional climate model over East Asia

Ui-Yong Byun[1,2], Eun-Chul Chang[1,2*], Joowan Kim[1,2], Joong-Bae Ahn[3], Dong-Hyun Cha[4], Seung-Ki Min[5], and Young-Hwa Byun[6]

[1]Department of Atmospheric Science, Kongju National University, Gongju, Republic of Korea.

[2]Earth Environment Research Center, Kongju National University, Gongju, Republic of Korea.

[3]Department of Atmospheric Sciences, Pusan National University, Busan, Republic of Korea.

[4]School of Urban & Environmental Engineering, Ulsan National Institute of Science and Technology, Ulsan, Republic of Korea.

[5]Division of Environmental Science and Engineering, Pohang University of Science and Technology, Pohang, Republic of Korea.

[6]Climate Change Research Team, National Institute of Meteorological Sciences, Jeju, Republic of Korea.

Corresponding author: Eun-Chul Chang (echang@kongju.ac.kr)

Key Points:

- Regional climate models improve accuracy of climate projections for East Asia by simulating local climates at higher resolution than global climate models Key.
- Regional climate models effectively evaluate potential impacts of climate change on specific regions and inform local adaptation strategies.
- The added value of regional climate models in improving global climate models' bias and agreement with high-resolution reanalysis in mountainous regions is shown.

Abstract

Studies have shown that regional climate models (RCMs) can simulate local climates at a higher resolution for specific regions compared to global climate models (GCMs), making dynamic downscaling using RCMs a more effective approach. Therefore, RCMs have become valuable tools for evaluating the potential impacts of climate change on specific regions and for informing local adaptation strategies. To fully understand the added value (AV) of RCMs, it is essential to understand how the characteristics differ between land and ocean. The complex topography of East Asia, including land and sea, makes it a suitable region for evaluating the AV of RCMs. In this study, we compared two regional simulations that integrated the same RCMs but employed different GCMs from the Coordinated Regional Climate Downscaling Experiment for their ability to simulate storm tracks in East Asia. The results of the RCMs over a historical period were compared with their host Coupled Model Intercomparison Project GCM projections and high-resolution reanalysis. In mountainous regions, the AV of the RCMs weakened the bias of the GCM and improved its agreement with the reanalysis. In plains and coastal areas, owing to the increase in horizontal resolution in RCMs, small-scale phenomena are well represented, and the storm track of RCMs shows similar values to that of the GCM in maritime regions. This study demonstrates the value of RCMs for improving the accuracy of climate projections in East Asia, informing adaptation strategies, and enhancing climate research.

Keywords: Added value, bandpass filter, regional climate model, WRF, CORDEX

Plain Language Summary

This study looked at how regional climate models can better simulate local climates in specific regions compared to global climate models. By analyzing storm tracks in East Asia, researchers compared regional climate models integrated with different global climate models to better understand the added value of regional climate models. The study found that the regional climate models improved the accuracy of global climate models over mountainous regions and brought them closer to high-resolution reanalysis. In the plains and coastal areas, the regional climate models accurately represented small-scale phenomena due to the increase in horizontal resolution. Overall, this study shows that regional climate models are valuable tools for evaluating climate change in specific regions and can provide more accurate predictions than global climate models alone. This research is essential for improving our understanding of how climate models work and can be used to better predict the future climate of different regions, which can help inform decision-making about mitigating climate change.

1 Introduction

Climate change can lead to numerous socioeconomic problems by shifting climatic conditions within regions. According to Hsiang et al. (2017), the economic loss caused by a 1 °C temperature increase reaches up to 1.2% of the total domestic product of the United States. Accurate climate projections and predictions of extreme weather events are essential for minimizing the social and economic losses caused by climate change. To obtain this information, international communities, centered on the Intergovernmental Panel on Climate Change (IPCC), support many scientific activities for climate projection. The Coupled Model Intercomparison Project (CMIP) of the World Climate Research Program (WCRP) is a core project that produces long-term climate projections based on state-of-the-art numerical models from multiple research organizations (Meehl et al., 1997; Taylor et al., 2012; Eyring et al., 2016). In addition, the recent

CMIP (CMIP6; Eyring et al., 2016) provides detailed climate simulations based on various emission scenarios from representative concentration pathways (RCPs; Moss et al., 2010) and shared socioeconomic pathways (SSPs; O'Neill et al., 2015).

Severe weather conditions due to climate change have become more frequent in recent years. Because global climate change scenarios are produced with a relatively coarse-resolution model configuration (approximately 100 km), capturing detailed regional climate characteristics is difficult. Regional climate model (RCMs), which apply a dynamic downscaling technique, have been widely used to determine detailed climatic characteristics that are not well represented in global climate models (GCMs) (Wang et al., 2004; Chang & Hong, 2011; Di et al., 2012; Lee & Hong, 2014; Gensini et al., 2015; Mezghani et al., 2017). The Coordinated Regional Climate Downscaling Experiment (CORDEX) framework, sponsored by the WCRP , is a representative program that examines regional climate information from various RCMs. Quality-controlled datasets for the regional climate change scenarios were produced using CORDEX. Recently, in the East Asia (EA) branch of CORDEX, regional climate change scenarios based on the CMIP5 and CMIP6 global climate change scenarios were produced using multi-RCMs.

In East Asia, atmospheric phenomena occur at various scales owing to the complex topography and lower boundary conditions, such as coastlines (Cha et al., 2011; Hong & Kanamitsu, 2014). Therefore, in this region, it is important to confirm small-scale phenomena that cannot be expressed in the global climate model (GCM) and assess the added value (AV) from the regional climate model (RCM). Analyzing the current climate using the dynamically downscaled results from the RCM is essential for evaluating the systematic error in the regional climate modeling process before assessing the future climate (Giorgi & Gutowski, 2015). In East Asia, various studies have been conducted to confirm the AV of RCM using current climate-change scenarios (Suh et al., 2012; Lee & Hong, 2014; Jin et al., 2016; Ahn et al., 2018; Kim et al., 2021). Lee and Hong (2014) examined the performance of extreme weather simulations in Korea at different RCM resolutions. The RCM performed better at capturing heavy rainfall and sweltering days as the resolution increased. Ahn et al. (2018) confirmed an improved dry bias near the Korean Peninsula in the RCM compared to the forcing data. Kim et al. (2021) showed that bias-corrected RCM results are similar to the observations. Despite these results, it is not easy to clearly identify whether AV in the RCM always enhance the quality of the downscaled results. The AV of the RCM has different effects depending on various factors such as the model, variable, scale, region, and experimental configuration. Therefore, confirming where and in which elements the AV appears (Rummukainen, 2016) is essential.

Precipitation systems over the Korean Peninsula are significantly affected by migrating extratropical cyclones throughout the year. Identifying the characteristics of individual cyclones that have a significant impact on the local climate can be accomplished by determining their activity. However, using a storm track (ST) to assess the overall characteristics of the cyclones is a more efficient approach. ST is expressed as the disturbances of a specific period associated with a synoptic-scale baroclinic wave and is used prominently in the East Asian regions (Chung et al., 1976; Whittaker & Horn, 1984; Chen et al., 2014). In the inland areas of East Asia, low pressure is actively generated by lee cyclogenesis on the windward side of mountain ranges, such as the Tibetan Plateau, resulting in solid ST intensity (Chung et al., 1979; Whittaker & Horn, 1984). Among the maritime regions of East Asia, cyclogenesis due to warm sea surface temperatures (SSTs) occur in the East China Sea and the Kuroshio extension region, which also affects the ST (Chen et al., 1991; Zhang et al., 2019). The cyclones formed by these factors

develop toward the Aleutian Islands. Owing to these characteristics, high cyclone variability occurs in the northwestern Pacific (NWP) region.

The Northwestern Pacific storm track (NWPST) which shows maximum values in winter, is inextricably linked to the weather and climate systems of the Northern Hemisphere. Heat, moisture, and angular momentum are redistributed by ST (Mbengue & Schneider, 2018). Variations in the intensity and location of the NWPST have a distinct impact on the regional climate of East Asia (Nakamura et al., 2002; Zhang et al., 2014; Yang et al., 2021). Nakamura et al. (2002) confirmed that the strengthening of NWPST intensity in the late 1980s weakened the northwesterly monsoon flow from the Siberian high to the Aleutian low region. Zhang et al. (2014) showed the meridional oscillation of the NWPST in the East Asian winter monsoon (EAWM) using empirical orthogonal function analysis. In addition, Yang et al. (2021) confirmed the relationship between EAWM strength and the zonal distribution of the NWPST. Enhanced cold air transport from high latitudes when the EAWM is enhanced can suppress the growth of transient eddies in the entrance region and weaken the WNPST intensity. These studies used global reanalysis data to focus on the relationship between the EAWM and NWPST. Although previous studies have focused on the relationship between the NWPST and the global climate system, there are limitations in clarifying a specific region's regional-scale climate characteristics. The characteristics of NWPST can be examined through dynamic downscaling methods using the RCM, which includes dynamic processes such as cyclogenesis, which can simulate regional-scale phenomena.

In this study, the winter ST over East Asia was analyzed using the dynamic downscaling results of the RCM performed with different GCM forcings, and the effects of the AV of RCMs were addressed.

2 Data and Methods

The RCM used in this study was the Weather Research and Forecasting (WRF) Model (Skamarock et al., 2008) version 3.7. The essential components of the physics package are as follows: the WRF single moment 6-class scheme (WSM6) for cloud microphysics (Hong and Lim, 2006), the rapid radiative transfer scheme for general circulation models (RRTMG) for shortwave and longwave radiation (Iacono et al., 2008), the Yonsei University (YSU) scheme for planetary boundary layers (Hong et al., 2006), and the Noah land surface model (Chen & Dudhia, 2001). The Max Planck Institute Earth System Model - Low Resolution (MPI-ESM-LR) (Giorgetta et al., 2013) from CMIP5 and United Kingdom Earth System Model 1 - Low Resolution (UKESM1-0-LL) (Sellar et al., 2019) from CMIP6 provided the initial and boundary conditions for the RCM every 6 h. The model domain for this study was centered at 34.40°N and 116.57°E, with a 25-km horizontal resolution and 33 sigma levels extending to a model top of 50 hPa, in accordance with the CORDEX East Asia phase 2 framework (see Fig. 1). Spectral nudging (Miguez-Macho et al., 2004) of the horizontal wind (U and V) was applied to retain large-scale information from the GCM during the integration of the WRF model. The large-scale structure was employed using two-dimensional Fourier low-pass filtering with threshold wavenumbers of 9 and 6 in the x- and y-directions, respectively, which allowed the nudging of GCM information larger than approximately 1000 km horizontally. The nudging coefficient is set to 0.0001 s^{-1}. In this study, 24 winters were analyzed from December 1981 to February 2005 for the entire model integration period of 1979–2005. The fifth-generation ECMWF's reanalysis

(ERA5) was used to evaluate the simulated results. The spatial resolution of the ERA5 data was approximately 31 km, and the vertical resolution was 137 km (Hersbach & Dee, 2016).

The intensity of the storm track was analyzed using bandpass filtering methods for five different datasets: two GCMs, two RCM results downscaled from different GCMs, and ERA5. Bandpass filtering is a valuable method because the resultant eddy quantities reflect the intimate interaction between transient eddies and the time-mean flow (Chang et al., 2002; Chang, 2009; Hoskins & Hodges, 2019). An ST is defined as a localized maximum in the transient bandpass variance (Blackmon, 1976). Through bandpass filtering methods, it is possible to analyze the variables at every atmospheric level and investigate the three-dimensional distribution of the storm track. This study used the Lanczos bandpass filtering method (Duchon, 1979) to selectively extract signals on a synoptic scale (2–7 d).

Denote the filtered time series at a grid point as x(t), and its Hilbert transform as $\hat{x}(t)$, which lags x(t) by π/2 phase, based on

$$\hat{x}(t) \approx \sum_{l=-L}^{L} x(t-l)h(l) \qquad (1)$$

$$h(l) = \begin{cases} \frac{2}{\pi l}\sin^2\left(\frac{\pi l}{2}\right), & l \neq 0 \\ 0, & l = 0 \end{cases}. \qquad (2)$$

Ideally L=∞ in (1), but in this study L=28, which provides an adequate amplitude response in the frequency domain (Barnett, 1983). After the Hilbert transform, the data for November 24–30 and March 1–7 are not available because of tapering. Hence, we only used data from the 90 d since December 1 in the following analysis.

3 Results

Figure 2 shows the average bandpass standard deviation (BPSD) of sea level pressure for December–January–February from 1982 to 2005. A high BPSD value in a region indicates an increased likelihood of cyclone activity, either due to frequent cyclogenesis or the movement of existing cyclones. The BPSD from ERA5 (Fig. 2a) showed intense activity over continental mountainous regions and maritime regions. A high BPSD of over 450 Pa was shown over Mongolia along the Altai–Sayan Mountains to the Gobi Desert, caused by lee cyclogenesis (Chen and Lazic, 1990). The Taklamakan Desert, between the Altai Mountains and Tibet, has a relatively low BPSD of approximately 200 Pa, owing to the suppressed development of storms. In the maritime region, it has been shown that much stronger cyclone activity (BPSD over 700 Pa) than on the continent is captured over the Northwest Pacific region, which is the eastern region of Kuril Island, owing to cyclogenesis caused by warm ocean currents (Chen et al., 1992). This high BPSD is a result of the characteristics of East Asian regional storms, which gradually develop and disappear as they move to the corresponding area.

The MPI showed an overall higher cyclone activity than ERA5 over the inland area (Fig. 2b), whereas the general features were similar to those of the reanalysis. For detailed features

over the Altai–Sayan Mountains, the MPI simulated more robust cyclone activity with a BPSD higher than 550 Pa, including in the Taklamakan Desert region, which showed a lower BPSD in the ERA5. In the Northeast China Plain, which is the mid-area of the two analyzed PBSD cores (i.e., the Altai–Sayan and Northwest Pacific regions), the MPI showed a higher ST intensity (>400 Pa) than the reanalysis (approximately 300 Pa). However, the UKESM did not distinctly capture the inland ST intensity over the Altai–Sayan area, as shown in ERA5 (Fig. 2c).

Figure 2d and 2e show the BPSD for the regional climate model using MPI and UKESM as the input data, respectively. Interestingly, the dynamic downscaling employed by each GCM significantly improved the bias that appeared in the inland areas. The WRF model, which used MPI global forcing data, showed a lower BPSD for sea level pressure than the GCM (Fig. 2d). This offset the negative BPSD bias of approximately 150 hPa in Mongolia and the surrounding GCM (Fig. 3a). In contrast, the opposite counterbalance appeared in the WRF model using UKESM data (Fig. 2e). This improved the positive bias of the GCM by approximately –120 hPa over the region from the Tibetan Plateau to the Gobi Desert (Fig. 3b). The GCM has limitations in expressing a low-pressure system caused by complex terrain owing to its low resolution. The ST of Mongolia was strongly or weakly simulated, depending on the topographic information used in the GCM. The GCM data were used only as lateral boundary conditions in the RCM, and the atmospheric conditions in the inner domain were calculated using their dynamic processes. Therefore, in the RCM, a dynamic expression such as lee cyclogenesis is improved because of the high-resolution topographic data used as the lower boundary condition. This enhanced the bias shown by the GCM, which was close to the observations. Unlike the inland area, where dramatic changes appeared, both RCMs showed a lower BPSD (approximately 25 hPa) than the GCM, regardless of the GCM bias in the ocean. This feature appeared because the energy flux conditions at the sea surface from the global model were applied in the RCM without significant changes in the case of the ocean region.

The BPSD of the meridional wind at 850 hPa is shown in Figure 4. These figures can be used to examine the momentum and energy transport from lower to higher altitudes due to the ST in the lower troposphere. However, small-scale phenomena expressed in ERA5 were not well resolved in the GCM, owing to its low resolution. Inland areas with complex topography, such as the Taklamakan Desert and Altai Mountains, did not express well in the BPSD values, and small-scale phenomena over inland China, such as the Sichuan Basin and Hubei Plain, were also not resolved. In contrast, in both the RCMs, characteristics similar to those of ERA5 were expressed in the corresponding regions. Small-scale phenomena on steep slopes around Tibet and inland China were decomposed and expressed. Low-pressure systems that cause heavy rainfall in East Asia, including the Korean Peninsula, are created and developed (Shin and Lee, 2015; Song et al., 2017). However, performing numerical modeling is challenging because of the unique flow structure over the steep slope of the eastern boundary of Tibet and the stagnation of the basin (Zhang et al., 2014).

Figure 5 shows the BPSD of the meridional eddy heat flux distribution, a typical feature of the Northwest Pacific region during the winter season. In ERA5, the BPSD of the heat flux core appeared in the Northwest Pacific region, with a central value of approximately 15 km s^{-1}. In the MPI, the central value is 12 km s^{-1}, which is lower than that of ERA5, and in the UKESM, it appears similar to that of ERA5. In the WRF model, the heat flux cores over this region are similar to the GCM forcing employed. Additionally, in ERA5, there was a high eddy heat flux region along the northern coastal part of the Korean Peninsula, such as the Gulf of Pohai and

Peter Great Bay. These two cores were simulated as one in both the MPI and UKESM results. However, in the WRF model, the small-scale feature of heat flux over the coastal region was represented. In particular, the high BPSD of the heat flux band from the Peter Great Bay to Japan is well expressed.

The time series of the BPSD of the sea level pressure is shown in Figure 6. To confirm the AV of the RCM, the analyzed regions marked in Figure 1 were established for the land and ocean areas. The land area is mainly composed of the Altai Mountains region, where AV are evident, and the ocean area is the Northwest Pacific region, including the Kuril Islands. The ocean area is located to the west of the area where the maximum BPSD statistics appear, but it is configured such that the area is less affected by the buffer zone. The annual variation in the BPSD of sea level pressure from the RCM shows similar behavior to that of the GCM. As shown in Figures 2 and 3, which are analyzed as the average values for the entire period, MPI overestimates the bandpass filtered value and UKESM underestimates it, respectively, compared to that in the ERA5 reanalysis data. The two WRF models that forced each GCM data point improved this bias despite having opposite directions. The average bias of the WRF model for UKESM is 36 Pa, and that for MPI is –62 Pa. This value appeared to be constant over the entire period. For the ocean, the bandpass statistics from both GCMs showed relatively similar ERA5 values. The simulated bandpass-filtered standard deviations of sea-level pressure values in the RCM were –11 Pa for UKESM and –20 Pa for MPI, which were lower than those for land.

4 Summary

This study provides evidence for the impact of the RCM AV on dynamical downscaling outcomes in the East Asian region. Two different GCMs (MPI for CMIP5 and UKESM for CMIP6) were compared by forcing the WRF model. The bandpass filtering method was used to separate the synoptic scale (2–7 d) to represent the storm track. The spectral nudging method was applied to all layers of the WRF data, except the planetary boundary layer, to ensure risk control during decades of integration. The RCM bandpass statistics in the middle- and upper-troposphere storm tracks were similar to those of the GCM (not shown). As a result, this study concentrates on surface and lower tropospheric storm tracks.

The AV of the RCM in East Asia differs depending on the region. The use of RCM AV in this study helped to reduce the bias of the GCM over inland high-altitude regions, such as the Tibetan Plateau or Mongolia, bringing the results closer to the reanalysis. These characteristics appear to result from the dynamic balance within the RCM due to the high-resolution lower boundary information, such as topography and land use land cover. Owing to the high-resolution surface information, dynamic phenomena, such as lee cyclogenesis, are well simulated in the RCM. In the eastern flank of the Tibetan Plateau and the coastal region, the characteristics of the AV due to the increase in horizontal resolution were well confirmed. Small-scale phenomena that are not expressed in the GCM are well represented. In the maritime region, the ST of the RCM was similar to that of the GCM. In the numerical model, the atmosphere over the ocean is sensitive to lower boundary conditions, such as surface temperature, as in nature (Kim and Hong, 2010). Unlike the land, which requires dynamic rebalancing, the lower atmosphere of the RCM is greatly affected by the lower boundary conditions of the GCM. According to previous studies, when high-resolution SST data is employed, the model simulates oceanic cyclogenesis well (Small et al., 2014; Zhang et al., 2019). As ocean fronts are clearly expressed in high-resolution SST data, the transient eddy heat and moisture fluxes in the lower layer are also well expressed,

and these effects influence the troposphere beyond the boundary layer. In the Northwest Pacific region, the importance of high-resolution SST is even more remarkable because there is a warm current that expresses oceanic eddies, such as the Kuroshio Current. Explosive cyclones that develop in the northwestern Pacific region during winter (Sanders and Gyakum, 1980; Roebber, 1984) are closely related to strong winds and extreme weather in East Asia (Kang et al., 2020). Therefore, it is important to use accurate and high-resolution SST data as input for the model. It is necessary to increase the resolution and elaborate on the lower boundary conditions to improve the AV of the RCM. In inland regions, the refinement of information, such as topography, soil, and vegetation is required. In the case of climate models older than a decade, a reliable scenario should be produced if the model considers surface information changes. Maritime areas require reliable ocean information. Unlike past reproduction experiments that can utilize high-resolution SST data, future climate change scenario production, which makes it impossible to use analysis data, can improve the performance of oceanic cyclogenesis simulations through an atmospheric-marine coupled model. The interactions between the ocean and atmosphere in the coupled model provide desirable information on the formation and development of cyclones.

Acknowledgments

This study was funded by the Korea Meteorological Administration Research and Development Program (grant no. KMI2020-01411). This work was also supported by a research grant from the Kongju National University in 2021.

Data availability statement

The model simulation data used in this study are available upon reasonable request from the authors, and will be publicly available at https://esg-dn1.nsc.liu.se/search/cordex. The ERA5 data can be downloaded at https://www.ecmwf.int/en/forecasts/dataset/ecmwf-reanalysis-v5.

References

Ahn, J. B., Choi, Y. W., & Jo, S. (2018). Evaluation of reproduced precipitation by WRF in the Region of CORDEX-East Asia phase 2. *Atmosphere*, *28*(1), 85-97. https://doi.org/10.14191/Atmos.2018.28.1.085

Blackmon, M. L. (1976). A climatological spectral study of the 500 mb geopotential height of the Northern Hemisphere. *Journal of the Atmospheric Sciences*, *33*(8), 1607-1623. https://doi.org/10.1175/1520-0469(1976)033<1607:ACSSOT>2.0.CO;2

Cha, D. H., Jin, C. S., Lee, D. K., & Kuo, Y. H. (2011). Impact of intermittent spectral nudging on regional climate simulation using Weather Research and Forecasting

model. *Journal of Geophysical Research: Atmospheres*, *116*(D10). https://doi.org/10.1029/2010JD015069

Chang, E. C., & Hong, S. Y. (2011). Projected climate change scenario over East Asia by a regional spectral model. *Journal of the Korean Earth Science Society*, *32*(7), 770-783. https://doi.org/10.5467/JKESS.2011.32.7.770

Chang, E. K., Lee, S., & Swanson, K. L. (2002). Storm track dynamics. *Journal of Climate*, *15*(16), 2163-2183. https://doi.org/10.1175/1520-0442(2002)015<02163:STD>2.0.CO;2

Chang, E. K. (2009). Are band-pass variance statistics useful measures of storm track activity? Re-examining storm track variability associated with the NAO using multiple storm track measures. *Climate Dynamics*, *33*(2-3), 277-296. https://doi.org/10.1007/s00382-009-0532-9

Chen, F., & Dudhia, J. (2001). Coupling an advanced land surface–hydrology model with the Penn State–NCAR MM5 modeling system. Part I: Model implementation and sensitivity. *Monthly Weather Review*, *129*(4), 569-585. https://doi.org/10.1175/1520-0493(2001)129<0569:CAALSH>2.0.CO;2

Chen, L., Tan, B., Kvamstø, N. G., & Johannessen, O. M. (2014). Wintertime cyclone/anticyclone activity over China and its relation to upper tropospheric jets. *Tellus A: Dynamic Meteorology and Oceanography*, *66*(1), 21889. https://doi.org/10.3402/tellusa.v66.21889

Chen, S. J., & Lazić, L. (1990). Numerical case study of the Altai-Sayan lee cyclogenesis over east Asia. *Meteorology and Atmospheric Physics*, *42*(3), 221-229. https://doi.org/10.1007/BF01314826

340 Chung, Y. S., Hage, K. D., & Reinelt, E. R. (1976). On lee cyclogenesis and airflow in the
341 Canadian Rocky Mountains and the East Asian Mountains. *Monthly Weather*
342 *Review*, *104*(7), 879-891. https://doi.org/10.1175/1520-
343 0493(1976)104<0879:OLCAAI>2.0.CO;2
344 Di Luca, A., de Elía, R., & Laprise, R. (2012). Potential for added value in precipitation
345 simulated by high-resolution nested regional climate models and observations.
346 *Climate Dynamics*, *38*(5-6), 1229-1247. https://doi.org/10.1007/s00382-011-1068-3
347 Duchon, C. E. (1979). Lanczos filtering in one and two dimensions. *Journal of Applied*
348 *Meteorology and Climatology*, *18*(8), 1016-1022. https://doi.org/10.1175/1520-
349 0450(1979)018<1016:LFIOAT>2.0.CO;2
350 Eyring, V., Bony, S., Meehl, G. A., Senior, C. A., Stevens, B., Stouffer, R. J., & Taylor, K. E.
351 (2016). Overview of the Coupled Model Intercomparison Project Phase 6 (CMIP6)
352 experimental design and organization. *Geoscientific Model Development*, *9*(5),
353 1937-1958. https://doi.org/10.5194/gmd-9-1937-2016
354 Gensini, V. A., & Mote, T. L. (2015). Downscaled estimates of late 21st century severe weather
355 from CCSM3. *Climatic Change*, *129*(1), 307-321. https://doi.org/10.1007/s10584-
356 014-1305-z
357 Giorgetta, M. A., Jungclaus, J., Reick, C. H., Legutke, S., Bader, J., Böttinger, M., ... & Stevens,
358 B. (2013). Climate and carbon cycle changes from 1850 to 2100 in MPI-ESM
359 simulations for the Coupled Model Intercomparison Project phase 5. *Journal of*
360 *Advances in Modeling Earth Systems*, *5*(3), 572-597.
361 https://doi.org/10.1002/jame.20038

362 Giorgi, F., & Gutowski Jr, W. J. (2015). Regional dynamical downscaling and the CORDEX
363 initiative. *Annual Review of Environment and Resources*, *40*, 467-490.
364 https://doi.org/10.1146/annurev-environ-102014-021217.
365 Hersbach, H., Bell, B., Berrisford, P., Hirahara, S., Horányi, A., Muñoz-Sabater, J., ... &
366 Thépaut, J. N. (2020). The ERA5 global reanalysis. *Quarterly Journal of the Royal*
367 *Meteorological Society*, *146*(730), 1999-2049. https://doi.org/10.1002/qj.3803
368 Hong, S. Y., & Lim, J. O. J. (2006). The WRF single-moment 6-class microphysics scheme
369 (WSM6). *Asia-Pacific Journal of Atmospheric Sciences*, *42*(2), 129-151.
370 https://doi.org/10.1007/s13143-016-0011-z
371 Hong, S. Y., Noh, Y., & Dudhia, J. (2006). A new vertical diffusion package with an explicit
372 treatment of entrainment processes. *Monthly Weather Review*, *134*(9), 2318-2341.
373 https://doi.org/10.1175/MWR3199.1
374 Hong, S. Y., & Kanamitsu, M. (2014). Dynamical downscaling: Fundamental issues from an
375 NWP point of view and recommendations. *Asia-Pacific Journal of Atmospheric*
376 *Sciences*, *50*(1), 83-104.
377 Hoskins, B. J., & Hodges, K. I. (2019). The annual cycle of Northern Hemisphere storm tracks.
378 Part I: Seasons. *Journal of Climate*, *32*(6), 1743-1760. https://doi.org/10.1175/JCLI-
379 D-18-0061.1
380 Hsiang, S., Kopp, R., Jina, A., Rising, J., Delgado, M., Mohan, S., ... & Houser, T. (2017).
381 Estimating economic damage from climate change in the United
382 States. *Science*, *356*(6345), 1362-1369. https://doi.org/10.1126/science.aal4369
383 Iacono, M. J., Delamere, J. S., Mlawer, E. J., Shephard, M. W., Clough, S. A., & Collins, W. D.
384 (2008). Radiative forcing by long-lived greenhouse gases: Calculations with the

385 AER radiative transfer models. *Journal of Geophysical Research: Atmospheres*, *113*(D13). https://doi.org/10.1029/2008JD009944

387 Jin, C. S., Cha, D. H., Lee, D. K., Suh, M. S., Hong, S. Y., Kang, H. S., & Ho, C. H. (2016). Evaluation of climatological tropical cyclone activity over the western North Pacific in the CORDEX-East Asia multi-RCM simulations. *Climate Dynamics*, *47*(3), 765-778. https://doi.org/10.1007/s00382-015-2874-8

391 Kang, J. M., Lee, J., Son, S. W., Kim, J., & Chen, D. (2020). The rapid intensification of East Asian cyclones around the Korean Peninsula and their surface impacts. *Journal of Geophysical Research: Atmospheres*, *125*(2), e2019JD031632. https://doi.org/10.1029/2019JD031632

395 Kim, E. J., & Hong, S. Y. (2010). Impact of air-sea interaction on East Asian summer monsoon climate in WRF. *Journal of Geophysical Research: Atmospheres*, *115*(D19). https://doi.org/10.1029/2010JD013892

398 Kim, G., Cha, D. H., Park, C., Jin, C. S., Lee, D. K., Suh, M. S., ... & Kang, H. S. (2021). Evaluation and projection of regional climate over East Asia in CORDEX-East Asia Phase I experiment. *Asia-Pacific Journal of Atmospheric Sciences*, *57*(1), 119-134. https://doi.org/10.1007/s13143-021-00224-6

402 Lee, J. W., & Hong, S. Y. (2014). Potential for added value to downscaled climate extremes over Korea by increased resolution of a regional climate model. *Theoretical and Applied Climatology*, *117*(3), 667-677. https://doi.org/10.1007/s00704-013-1021-1

405 Mbengue, C., & Schneider, T. (2018). Linking Hadley circulation and storm tracks in a conceptual model of the atmospheric energy balance. *Journal of the Atmospheric Sciences*, *75*(3), 841-856. https://doi.org/10.1126/science.aba9757

Meehl, G. A., Boer, G. J., Covey, C., Latif, M., & Stouffer, R. J. (1997). Intercomparison makes for a better climate model. *Eos, Transactions American Geophysical Union*, *78*(41), 445-451. https://doi.org/10.1029/97EO00276

Mezghani, A., Dobler, A., Haugen, J. E., Benestad, R. E., Parding, K. M., Piniewski, M., ... & Kundzewicz, Z. W. (2017). CHASE-PL Climate Projection dataset over Poland–bias adjustment of EURO-CORDEX simulations. *Earth System Science Data*, *9*(2), 905-925. https://doi.org/10.5194/essd-9-905-2017

Moss, R. H., Edmonds, J. A., Hibbard, K. A., Manning, M. R., Rose, S. K., Van Vuuren, D. P., ... & Wilbanks, T. J. (2010). The next generation of scenarios for climate change research and assessment. *Nature*, *463*(7282), 747-756. https://doi.org/10.1038/nature08823

Nakamura, H., Izumi, T., & Sampe, T. (2002). Interannual and decadal modulations recently observed in the Pacific storm track activity and East Asian winter monsoon. *Journal of Climate*, *15*(14), 1855-1874. https://doi.org/10.1175/1520-0442(2002)015<1855:IADMRO>2.0.CO;2

O'Neill, S., & O'Driscoll, L. (2015). Metabolic syndrome: a closer look at the growing epidemic and its associated pathologies. *Obesity Reviews*, *16*(1), 1-12. https://doi.org/10.1111/obr.12229.

Roebber, P. J. (1984). Statistical analysis and updated climatology of explosive cyclones. *Monthly Weather Review*, *112*(8), 1577-1589. https://doi.org/10.1175/1520-0493(1984)112<1577:SAAUCO>2.0.CO;2

Rummukainen, M. (2016). Added value in regional climate modeling. *Wiley Interdisciplinary Reviews: Climate Change*, *7*(1), 145-159. https://doi.org/10.1186/s40562-022-00247-6

Sanders, F., & Gyakum, J. R. (1980). Synoptic-dynamic climatology of the "bomb". *Monthly Weather Review*, *108*(10), 1589-1606. https://doi.org/10.1175/1520-0493(1980)108<1589:SDCOT>2.0.CO;2

Skamarock, W. C., & Klemp, J. B. (2008). A time-split nonhydrostatic atmospheric model for weather research and forecasting applications. *Journal of Computational Physics*, *227*(7), 3465-3485. https://doi.org/10.1016/j.jcp.2007.01.037

Sellar, A. A., Jones, C. G., Mulcahy, J. P., Tang, Y., Yool, A., Wiltshire, A., ... & Zerroukat, M. (2019). UKESM1: Description and evaluation of the UK Earth System Model. *Journal of Advances in Modeling Earth Systems*, *11*(12), 4513-4558. https://doi.org/10.1029/2019MS001739

Shin, U., & Lee, T. Y. (2015). Origin, evolution and structure of meso-α-scale lows associated with cloud clusters and heavy rainfall over the Korean peninsula. *Asia-Pacific Journal of Atmospheric Sciences*, *51*(3), 259-274. https://doi.org/10.1007/s13143-015-0076-3

Small, R. J., Tomas, R. A., & Bryan, F. O. (2014). Storm track response to ocean fronts in a global high-resolution climate model. *Climate Dynamics*, *43*(3), 805-828. https://doi.org/10.1007/s00382-013-1980-9

Song, I. S., Byun, U. Y., Hong, J., & Park, S. H. (2018). Domain-size and top-height dependence in regional predictions for the Northeast Asia in spring. *Atmospheric Science Letters*, *19*(1), e799. https://doi.org/10.1002/asl.799

Suh, M. S., Oh, S. G., Lee, D. K., Cha, D. H., Choi, S. J., Jin, C. S., & Hong, S. Y. (2012). Development of new ensemble methods based on the performance skills of regional climate models over South Korea. *Journal of Climate*, *25*(20), 7067-7082. https://doi.org/10.1175/JCLI-D-11-00457.1

Taylor, K. E., Stouffer, R. J., & Meehl, G. A. (2012). An overview of CMIP5 and the experiment design. *Bulletin of the American Meteorological Society*, *93*(4), 485-498. https://doi.org/10.1175/BAMS-D-11-00094.1

Wang, Y., Leung, L. R., McGregor, J. L., Lee, D. K., Wang, W. C., Ding, Y., & Kimura, F. (2004). Regional climate modeling: progress, challenges, and prospects. *Journal of the Meteorological Society of Japan. Ser. II*, *82*(6), 1599-1628. https://doi.org/10.2151/jmsj.82.1599

Whittaker, L. M., & Horn, L. H. (1984). Northern Hemisphere extratropical cyclone activity for four mid-season months. *Journal of Climatology*, *4*(3), 297-310. https://doi.org/10.1002/joc.3370040307

Yang, M., Li, C., Li, X., Tan, Y., Chen, X., & Zhang, C. (2021). Interdecadal Change in the Relationship between the Winter North Pacific Storm Track and the East Asian Winter Monsoon. *Journal of Climate*, *34*(8), 3171-3187. https://doi.org/10.1175/JCLI-D-20-0372.1

Zhang, M., Qi, Y., & Hu, X. M. (2014). Impact of East Asian winter monsoon on the P acific storm track. *Meteorological Applications*, *21*(4), 873-878. https://doi.org/10.1002/met.1423

Zhang, P., Li, G., Fu, X., Liu, Y., & Li, L. (2014). Clustering of Tibetan Plateau vortices by 10–30-day intraseasonal oscillation. *Monthly Weather Review*, *142*(1), 290-300.

https://doi.org/10.1175/MWR-D-13-00137.1

Zhang, X., Ma, X., & Wu, L. (2019). Effect of mesoscale oceanic eddies on extratropical cyclogenesis: A tracking approach. *Journal of Geophysical Research: Atmospheres*, *124*(12), 6411-6422. https://doi.org/10.1029/2019JD030595

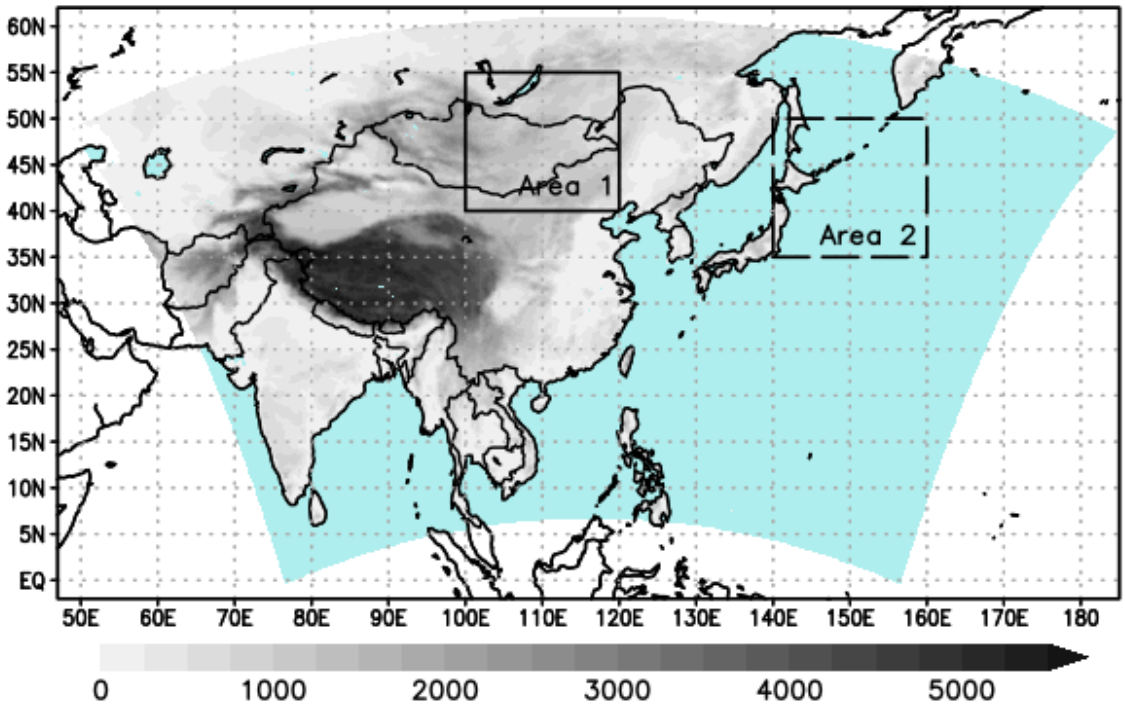

Figure 1. Regional model domain and terrain height shaded every 200 m.

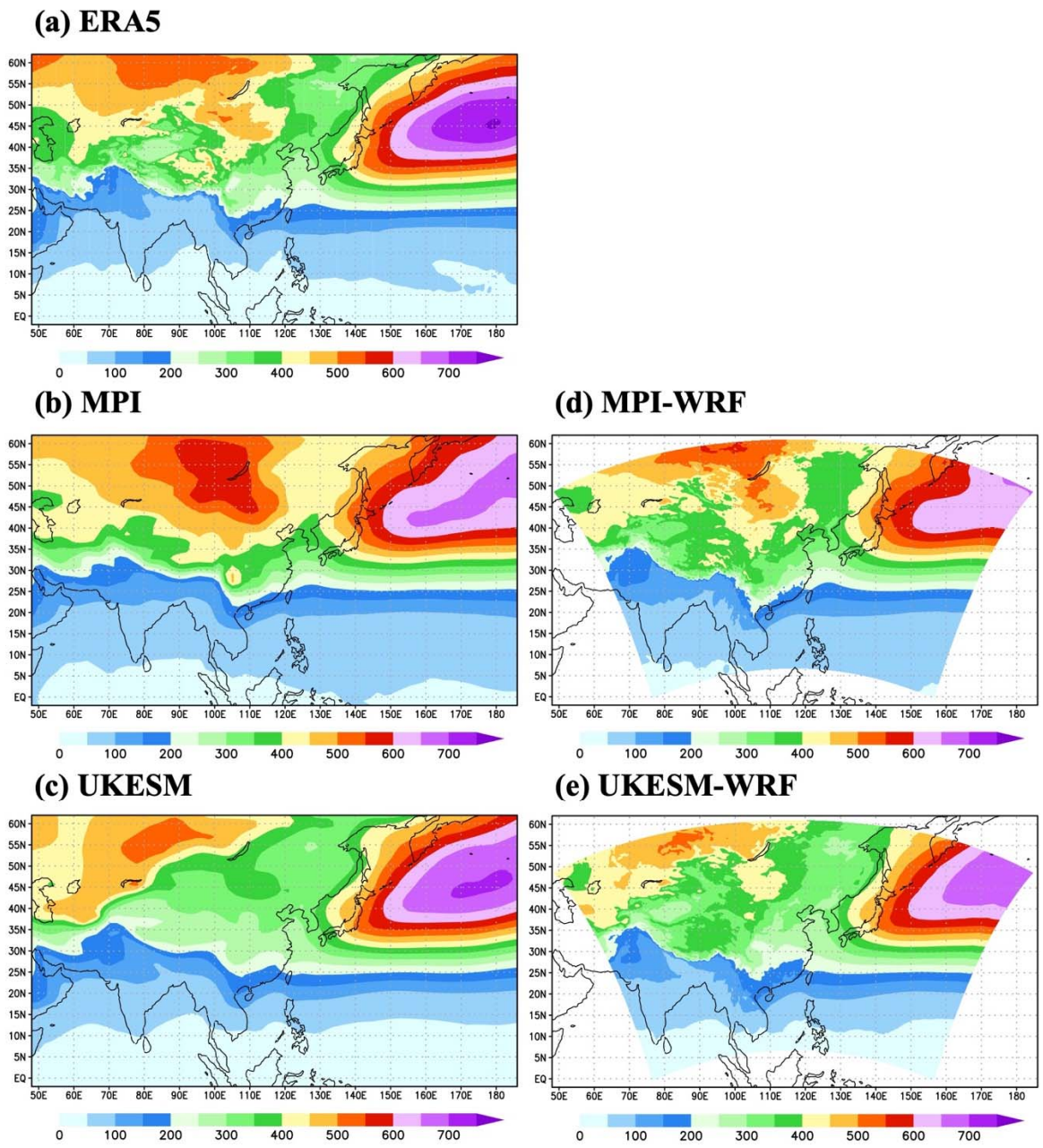

Figure 2. Averaged fields for December–January–February from 1982 to 2005 for the bandpass standard deviations of sea level pressure from the (a) ERA5 analysis, (b) MPI-ESM-LR, (c) UKESM, (d) WRF forced MPI, and (e) WRF forced UKESM (unit: hPa).

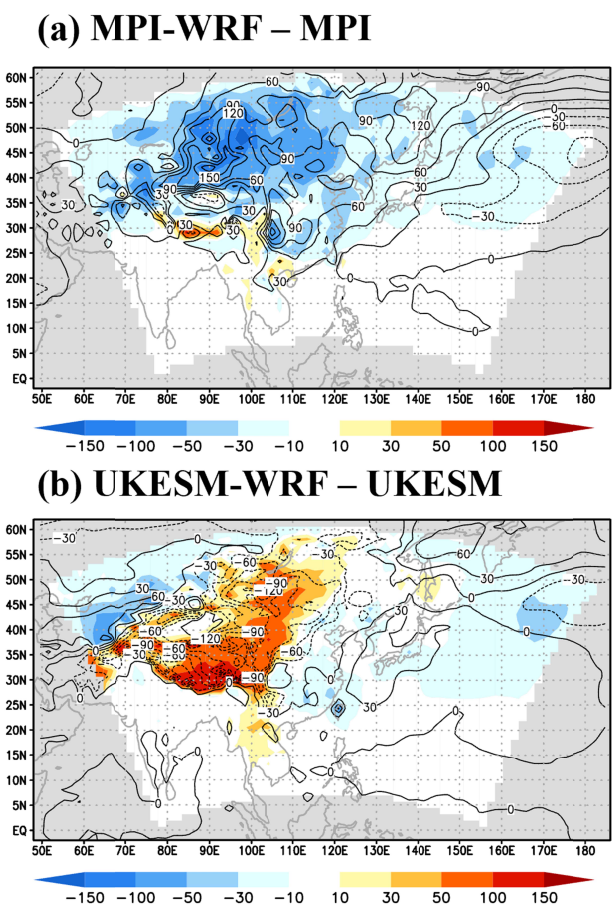

Figure 3. Bandpass standard deviation bias of WRF model regarding employed forcing GCM (shading) (a) MPI, and (b) UKESM. The contours denote the bandpass standard deviation bias of GCM about ERA5 reanalysis.

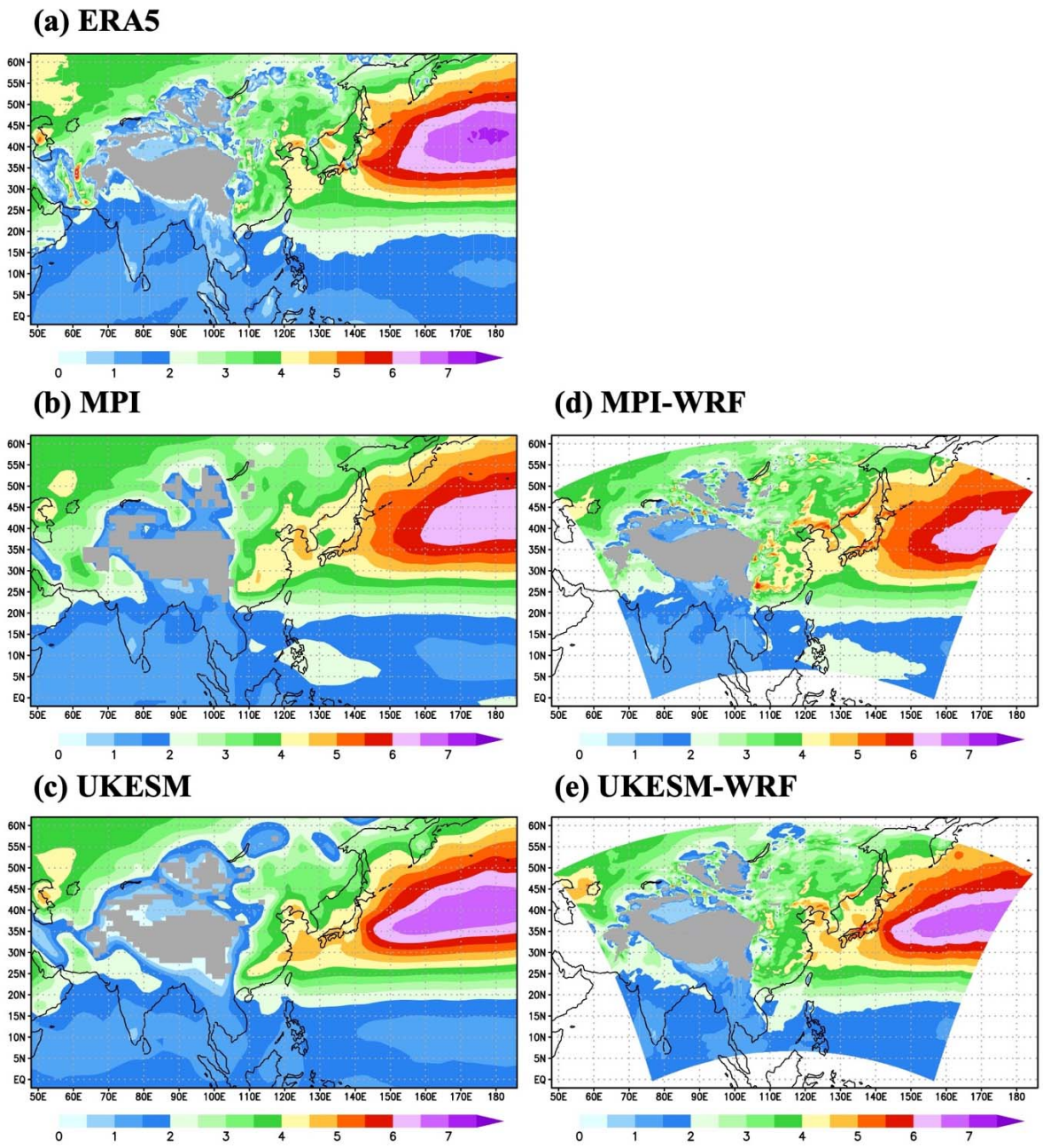

491
492 **Figure 4**. Same as Figure 2 but for the meridional wind at 850 hPa (unit: m s^{-1}).
493

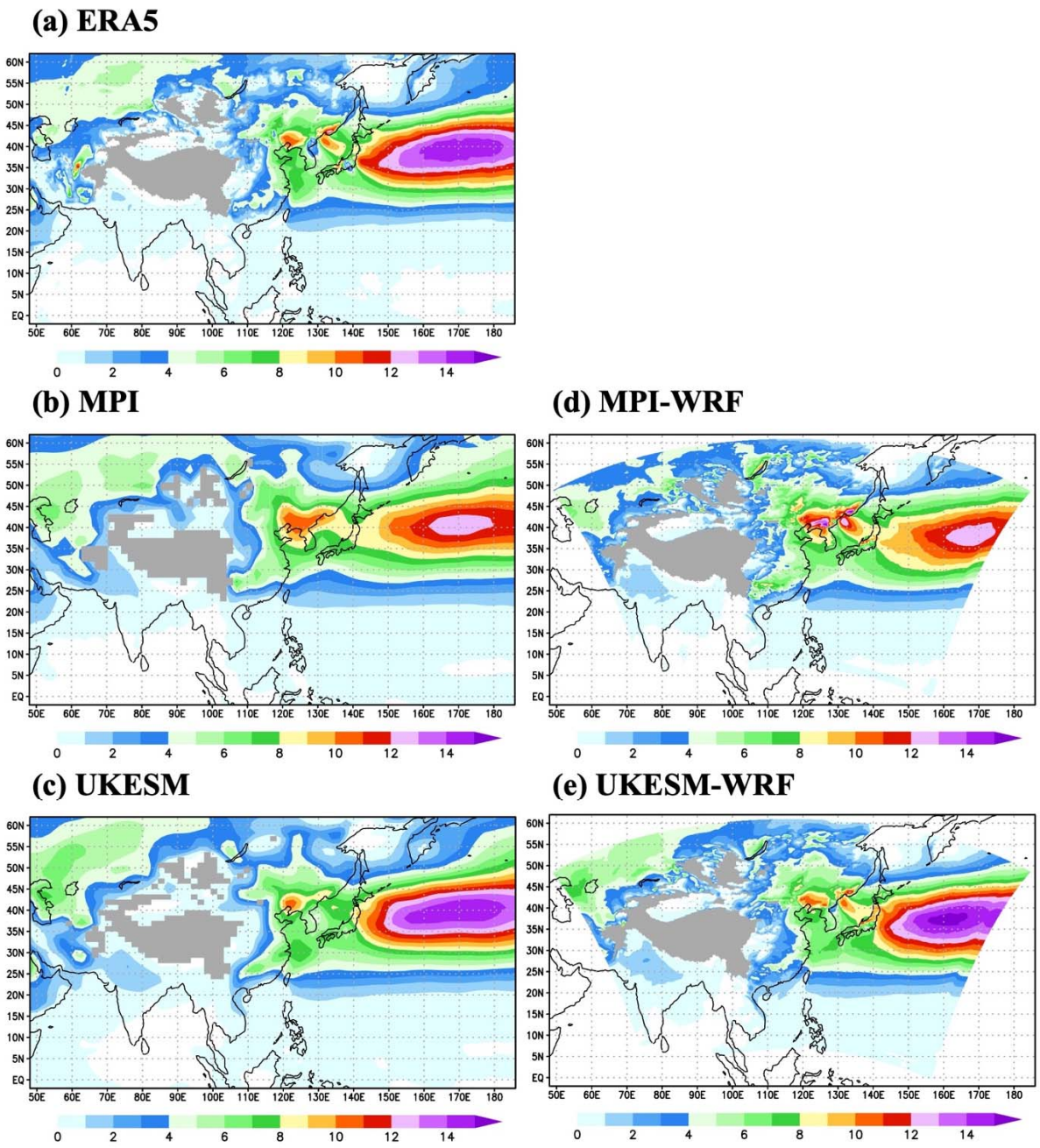

494
495 **Figure 5.** Same as Figure 2 but for the meridional eddy heat flux at 850 hPa (unit: km s^{-1}).
496

(a)

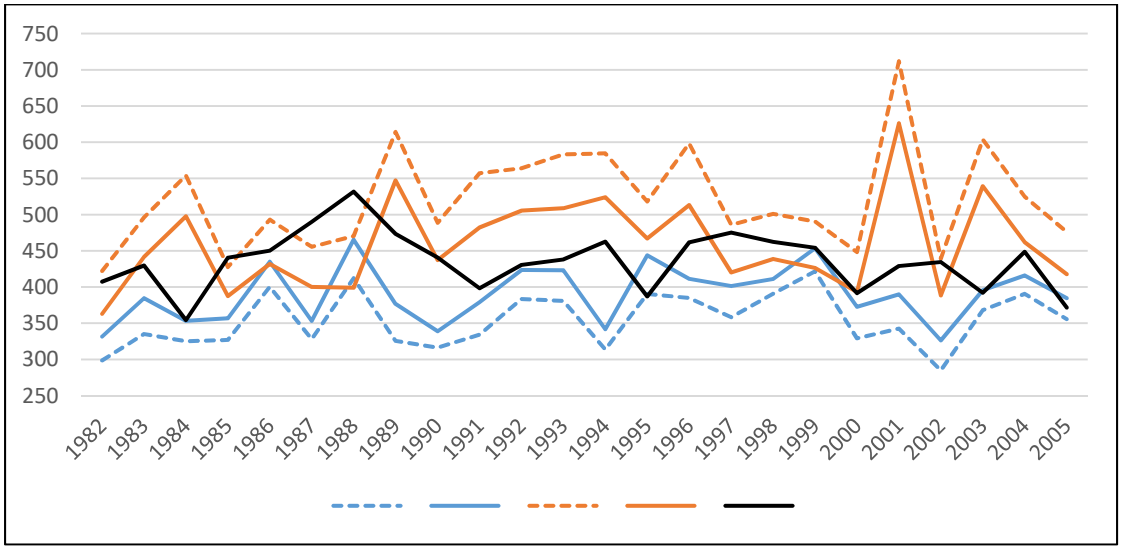

(b)

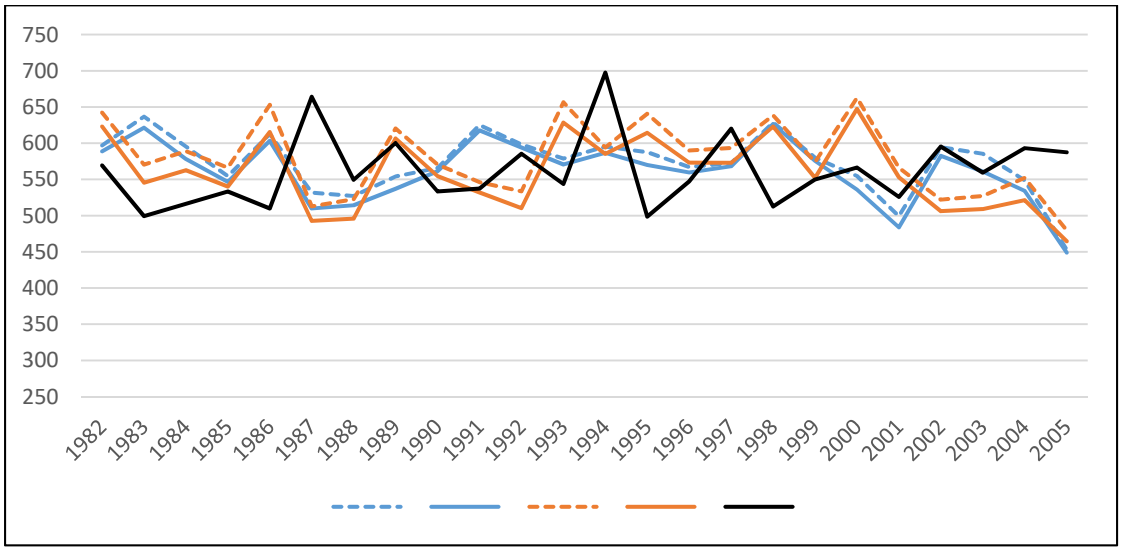

Figure 6. Time series of bandpass standard deviations of sea level pressure which are presented for the (a) inland region marked as a solid box and (b) marine region marked as a dashed box in Fig. 1.